
Detecting Adversarial Examples using Neural Fingerprinting

Sumanth Dathathri*
Caltech
sdathath@caltech.edu

Stephan Zheng*†
Salesforce Research
stephan.zheng@salesforce.com

Tianwei Yin
University of Texas at Austin
yintianwei@utexas.edu

Yisong Yue
Caltech
yyue@caltech.edu

Richard M. Murray
Caltech
murray@cds.caltech.edu

Abstract

Deep neural networks are vulnerable to adversarial examples: input data that has been manipulated to cause dramatic model output errors. To address this challenge, we propose *NeuralFingerprinting (NFP)*: a simple, yet effective method to detect adversarial examples (in the grey-box and black-box threat models) for image data. *NFP* relies on verifying whether prediction behavior is consistent with a set of *fingerprints*. These fingerprints are encoded into the prediction response around the data-distribution during training, and are inspired by biometric and cryptographic signatures, and we provide a theoretical characterization of *NFP* for linear networks. We also show that *NFP* significantly improves on state-of-the-art adversarial detection mechanisms for deep neural networks, by detecting a full range of known adversarial attacks with 98-100% AUC-ROC scores on the MNIST, CIFAR-10 and MiniImagenet (20 classes) datasets. We analyze *NFP* in detail under the grey/black-box threat models, when the adversary has limited or no-access to the exact fingerprints. Further, in the white-box setting, we find that *NFP* is robust against a full-array of the strongest-known attacks that have full knowledge of the defense; we subsequently developed a new adaptive white-box attack to fool *NFP*.

1 Introduction

Deep neural networks (DNNs) are highly effective pattern-recognition models for a wide range of tasks, e.g., computer vision [1], speech recognition [2] and sequential decision-making [3]. However, DNNs are vulnerable to adversarial examples: an attacker can add (small) perturbations to input data that are imperceptible to humans, and can drastically change the model's output, introducing catastrophic errors [4, 5, 6]. When DNNs encounters adversarial data, one desirable response is to flag the data and abstain from making confident predictions, thereby enabling DNNs to function reliably in noisy environments or mission-critical applications, e.g., in autonomous vehicles.

In this work, we study the problem of detecting adversarial data (after which the DNN abstains from making predictions). We propose *NeuralFingerprinting (NFP)*: a fast and secure method to training DNNs to robustly detect *grey-box* and *black-box* adversarial attacks [7]. The grey-box setting is motivated by the practical security setting where a private key is used to secure the system from adversaries [8]. For *NFP*, this specific key is the exact sequence of randomly generated fingerprints.

*Equal contribution.

†Work done while at Caltech.

The core idea of *NFP* is to encode fingerprint patterns into the response of a DNN around real data. These patterns characterize the DNN’s expected behavior around real data and can be used to detect adversarial examples. This approach is attractive as encoding fingerprints is simple to implement during training, and evaluation is computationally inexpensive. Furthermore, *NFP* is agnostic of the adversary’s attack mechanism. We provide a formal characterization of *NFP* for linear classification.

We conduct a thorough empirical evaluation of *NFP* across a range of adversarial attacks in computer vision. We show that *NFP* achieves state-of-the-art near-perfect AUC-ROC scores on detecting and separating unseen test data and adversarial examples in the grey- and black-box threat models. The performance of *NFP* is demonstrated to be robust to the choice of fingerprints and hyperparameters. Finally, we find that *NFP* is robust to a full-range previously known white-box adversarial attacks; we subsequently developed a new adaptive white-box attack to break *NFP* (See Appendix F).

2 Related Work

Detection versus Robust Prediction There are two broad classes of approaches to safe-guarding against adversarial data: robust prediction and detection. A major bottleneck with robust predictions can be the inherently larger sample complexity associated with robust learning [9]. Further, in [10], the authors argue that true robustness leads to depreciation in accuracy.

Robust Prediction of Adversarial Examples Several defenses based on robust learning have been proposed [11, 12, 13]. While these defenses provide robustness in the threat models (l_∞ bounded attacks) under which training is performed, the robustness does not carry over to other threat-models (bounded l_0, l_1 distortions [14], attacks with generative models [15]).

Several other defenses attempt to make robust predictions: by relying on randomization [16], introducing non-linearity that is not differentiable [17] and by relying on Generative Adversarial Networks [18, 19] for denoising images. However, recent work has shown that several of these defenses are not secure [20, 21, 22]. Several defenses proposed in the grey-box setting [23, 24] have been rendered vulnerable by attacking proxy defenses [25], ensembles and attacking the expectation over the distribution (for defenses relying on randomization) [20]. We study *NFP* extensively under these attacks and find that *NFP* is robust to such adaptive grey-box attacks.

Robust Detection of Adversarial Examples Amongst defenses that study the detection of adversarial examples, [26] detects adversarial samples using an auxiliary classifier trained to use an expansion-based measure, *local intrinsic dimensionality (LID)*. Similar detection methods based on Kernel Density (KD), Bayesian-Uncertainty (BU) [27] and the Mahalanobis Distance (MD) [28] using artifacts from trained networks have been considered. In contrast to such methods (including [23]), *NFP* does not need auxiliary classifiers and performs significantly better than LID, KD and BU when the attack mechanism is unknown.

Adversarial Attacks in Other Domains. We evaluate *NFP* on computer vision tasks, a domain in which DNNs have proved to be effective and adversarial examples have been extensively studied. *NFP* could potentially be employed to secure DNNs against attacks in domains such as speech recognition [29] and text comprehension [30]. Adversarial attacks have also been studied in domains such as detection of malware [31], spam [32] and intrusions [33]. Data-poisoning [34] is another form of attack where maliciously crafted data is injected during training.

3 Neural Fingerprinting

We consider supervised classification, where we aim to learn a model $f(x; \theta)$ from *real* data $\{(x^i, y^{*i})\}_{i \in \mathcal{I}}$, where $x \in \mathbb{R}^l$ is an input example (e.g., an image) and y^* is a 1-hot label vector $y^* \in \{0, 1\}^K$ over K classes. Here, we assume the data is sampled from a data distribution $P_{data}(x, y)$. For example, a neural network f predicts class probabilities $P(y|x; \theta)$ as:

$$f(x; \theta)_j = P(y_j|x; \theta) = \frac{\exp h(x; \theta)_j}{\sum_l \exp h(x; \theta)_l}, \quad (1)$$

where $h(x; \theta) \in \mathbb{R}^K$ are called logits and the most likely class is chosen. The optimal θ^* can be learned by minimizing a loss function $L(x, y; \theta)$, e.g., cross-entropy loss.

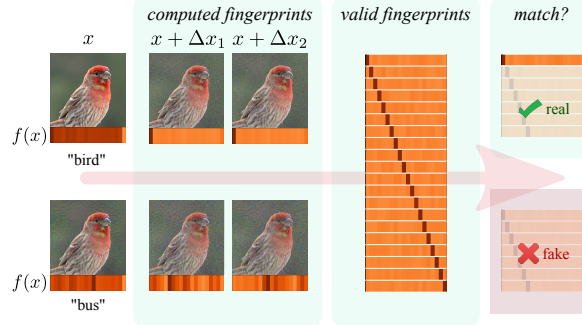


Figure 1: Example of detecting adversarial examples using *NFP* with $N = 2$ fingerprints, for K -class classification. $\varphi(x)$ is the model output. *NFP* separates real data x (top) from adversarial data $x' = x + \eta$ (bottom) by comparing the sensitivity of the model to predefined perturbations around unseen inputs with a reference sensitivity encoded around the manifold of *real* images during training. The training for *NFP* forces the maximum softmax scores on in-distribution samples to be high, and a threshold on the maximum softmax score distinguishes between real examples from adversarial.

Adversarial Attacks In an adversarial setting, an attacker attempts to construct adversarial examples x' , such that $\hat{y} = \operatorname{argmax}_l P(y_l | x'; \theta)$ is an *incorrect* class prediction (i.e., $P_{data}(x', \hat{y}) = 0$). In this work, we focus on *bounded* adversarial attacks, which produce small perturbations η that cause mis-classification. This is a standard threat model, for an extensive review see [35]. More generally, a bounded adversarial example causes a large change in model output, i.e. for $\delta, \rho > 0$, $\|\eta\| \leq \delta$, we have $\|f(x + \eta) - f(x)\| > \rho$ such that the class predicted by the model changes: $\operatorname{argmax}_j f(x + \eta)_j \neq \operatorname{argmax}_j f(x)_j$. An example bounded attack is the Fast-Gradient Sign Method (FGSM) [6] which uses an input-space gradient: $\eta \propto \operatorname{sign} \frac{\partial L(x, y; \theta)}{\partial x}$. Since the perturbation η is small, a perturbed image x' can be indistinguishable from x but still cause very different predictions.

Encoding Fingerprints into Network Response To defend DNNs against adversarial data, we propose training networks with *NFP*. Training with *NFP* entails encoding fingerprints around the data-distribution into the network response, and the network response can then be leveraged to detect whether an input example x is real or adversarial. A defender using *NFP* begins by choosing input perturbation(s) Δx around x , and desired changes in the model response Δy . Formally, we define a fingerprint χ as the tuple $\chi \triangleq (\Delta x, \Delta y)$. For K -class classification, we define a set of N fingerprints:

$$\chi^{i,j} = (\Delta x^i, \Delta y^{i,j}), \quad i = 1, \dots, N, \quad j = 1, \dots, K, \quad (2)$$

where $\chi^{i,j}$ is the i^{th} fingerprint for class j . To characterize sensitivity, we define the function $F(x, \Delta x^i)$ to measure the change in model output. A simple choice could be $F(x, \Delta x^i) = f(x + \Delta x^i) - f(x)$ (although we will use variations hereafter). Once a defender has constructed a set of desired fingerprints χ , the chosen fingerprints can be embedded into the network's response by adding a fingerprint regression loss during training. Given a classification model, the fingerprint loss is:

$$L_{\text{fp}}(x, y, \chi; \theta) = \sum_{i=1}^N \|F(x, \Delta x^i) - \Delta y^{i,k}\|_2^2, \quad (3)$$

where k is the ground truth class for example x and $\Delta y^{i,k}$ are the fingerprint outputs. Note that we *only train on the fingerprints for the ground truth class*. The total training objective then is:

$$\min_{\theta} \sum_{(x,y)} (L_0(x, y; \theta) + \alpha L_{\text{fp}}(x, y, \chi; \theta)), \quad (4)$$

where L_0 is a loss function (e.g. cross-entropy loss for classification) and α a positive scalar. Hereafter, we will use $\alpha = 1$ for brevity, but in practice, we choose α to balance the task and fingerprint losses. As noted before, the Δx^i ($\Delta y^{i,j}$) are chosen by the defender. Note that we use the same directions Δx^i for each class $j = 1, 2, \dots, K$, and that $\Delta y^{i,j}$ can be either discrete or continuous depending on $f(x; \theta)$. Here, the goal of a defender is to minimize $D(x, f, \chi^{i,j})$ for real data x .

Detecting Adversarial Examples We exploit the characterization described above to detect adversarial examples by comparing $F(x, \Delta x^i)$ with the reference output-perturbation Δy^i :

$$D(x, f, \chi^{\cdot j}) \triangleq \frac{1}{N} \sum_{i=1}^N \|F(x, \Delta x^i) - \Delta y^{i,j}\|_2. \quad (\text{comparison function}) \quad (5)$$

The objective from (4) trains the model so that the function D has low values around the real data, e.g., the train-set. The approach for detecting adversarial examples is summarized in Algorithm 1 and Figure 1. The key idea is to detect adversarial examples by using a *consistency check of the model output around the input*. *NFP* classifies a new input x' as *real* if the change in model output is close to the $\Delta y^{i,j}$ for some class j , for all i . Here, we use D and threshold $\tau > 0$ to define the level of agreement required, i.e., we declare x' *real* when D is below a threshold τ :

$$x' \text{ is real} \Leftrightarrow \exists j : D(x', f, \chi^{\cdot j}) \leq \tau. \quad (6)$$

Hence, the *NFP* test is defined by: $\text{NFPdata} = \left(\{\chi^{i,j}\}_{i=1\dots N, j=1\dots K}, D, \tau \right)$.

Computational Complexity Extra computation comes from checking the condition in (6) which requires $O(NK)$ forward passes to compute $F(x, \Delta x^i)$. A straightforward implementation is to check (6) iteratively, and stop whenever an agreement is seen or all classes have been exhausted. One can also parallelize the computation and use minibatches for real-time applications.

3.1 Choosing and Characterizing Fingerprints: Linear Models

We first analyze *NFP* on binary classification with data $\{(x^i, y^{*i})\}_{i \in \mathcal{I}}$ and linear model (SVM):

$$f(x) = \langle w, x \rangle + b, \quad \hat{y} = \text{sign } f(x) \in \{-1, 1\},$$

on inputs $x^i \in \mathbb{R}^n$, where $n \gg 1$ (e.g., $n = 900$ for MNIST). The SVM defines a hyperplane $f(x) = 0$ to separate positive ($\hat{y} = +1$) from negative examples ($\hat{y} = -1$). We will assume that the positive and negative examples are linearly separable by a hyperplane defined by a normal $\hat{w} = \frac{w}{\|w\|}$. We define the minimal and maximal distance from the examples to the hyperplane along \hat{w} as:

$$\delta_{\pm}^{\min} = \min_{i: y^i = \pm 1} |\langle x^i, \hat{w} \rangle|, \quad \delta_{\pm}^{\max} = \max_{i: y^i = \pm 1} |\langle x^i, \hat{w} \rangle|.$$

In this setting, the set of x^i classified as real by fingerprints is determined by the geometry of $f(x)$. Here, for detection, we measure the *exact change in predicted class* using:

$$F(x, \Delta x) = \Delta y = \text{sign}(\langle w, x + \Delta x \rangle + b) - \text{sign}(\langle w, x \rangle + b) \in \{-2, 0, 2\}.$$

Theorem 1 (Fingerprints for SVM). *Consider an SVM with $\hat{w} = \frac{w}{\|w\|}$ and separable data, and the following:*

$$(\Delta x^1 = \delta_{-}^{\min} \hat{w}, \Delta y^{1,-} = 0), \quad (7)$$

$$(\Delta x^2 = \delta_{-}^{\max} \hat{w}, \Delta y^{2,-} = +2), \quad (8)$$

$$(\Delta x^3 = -\delta_{+}^{\max} \hat{w}, \Delta y^{3,+} = -2), \quad (9)$$

$$(\Delta x^4 = -\delta_{+}^{\min} \hat{w}, \Delta y^{4,+} = 0). \quad (10)$$

Algorithm 1 NeuralFP

- 1: **inputs:** example x , model f , comparison func. D (Eq. 5), threshold $\tau > 0$, fingerprints $\{\chi^{i,j}\}$ (Eq. 2)
 - 2: **if** $\exists j : D(x, f, \chi^{\cdot j}) \leq \tau$ **then**
 - 3: **return:** accept *#real*
 - 4: **end if**
 - 5: **return:** reject *#fake*
-

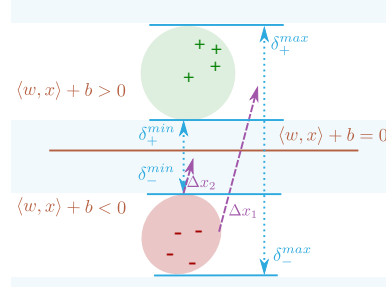


Figure 2: Geometry of fingerprints for SVMs with linearly separable data. Let $d(x)$ be the signed distance to the decision boundary (see Thm 1), and δ_{\pm}^{\max} (δ_{\pm}^{\min}) denote the maximal (minimal) distances of the positive (x_+) and negative (x_-) examples to the hyperplane $\langle w, x \rangle + b = 0$. The fingerprint Δx^1 with $\langle \Delta x^1, \hat{w} \rangle = \delta_{-}^{\min}$ will have $f(x_- + \Delta x) < 0$ and $f(x_-) < 0$ for all x_- in the data distribution (red region). Hence, Δx^1 will flag all x' in the regions $-\delta_{-}^{\min} < d(x') < 0$ as not real, since for those x' it will *always* see a change in predicted class. Similarly, Δx^2 with $\langle \Delta x^2, \hat{w} \rangle = \delta_{-}^{\max}$ always sees a class change for real x_- , flagging all $x' : d(x') < -\delta_{-}^{\max}$ as not real.

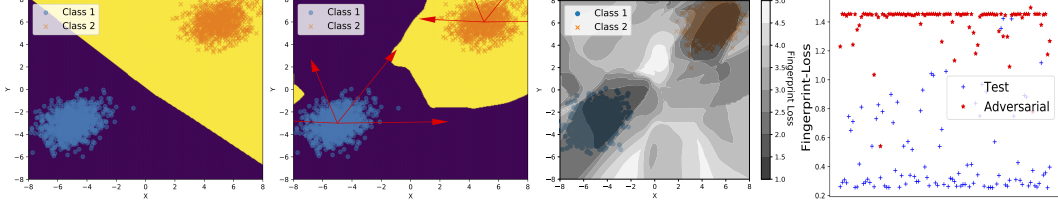


Figure 3: Left to right: 1) decision boundary without fingerprints. 2) with fingerprints, red arrows indicate fingerprint-directions. The decision boundary is more non-linear. 3) contour plot of fingerprint loss. *NFP* detects dark regions as “real”, while lighter ones are “fake” (tunable through τ). Fingerprinting creates valleys of low-loss delineating real data. 4) We see a similar phenomenon for the CIFAR-10 dataset. Fingerprint losses on 100 random test (blue) and adversarial (red) images (Table 3). We see a clear separation, illustrating that *NFP* is effective across many thresholds τ .

An adversarial input $x' = x_{\pm} + \eta$ is one for which one of the following holds:

$$d(x') > \delta_+^{max}, \quad 0 < d(x') < \delta_+^{min}, \quad d(x') < -\delta_-^{max}, \quad -\delta_-^{min} < d(x') < 0. \quad (11)$$

Here, $d(x') = \frac{\langle x', w \rangle + b}{\|w\|}$ is the signed distance to the separating hyperplane.

The proof for two fingerprints is shown in Figure 2. The full proof is in the Appendix. Theorem 1 by itself *does not* detect adversarial inputs that involve distortions *parallel* to the decision boundary. An adversary could push a negative example x_- across the boundary to a region outside the data distribution ($P_{data}(x_- + \eta, y) = 0$), but within distances δ_+^{min} and δ_+^{max} of the boundary. This would still be judged as real by using fingerprints. However, such examples could still be detected by also checking the distance of $x_- + \eta$ to the nearest x_+ in the dataset.

3.2 Choosing and Characterizing Fingerprints: DNNs

In contrast to the linear setting, in general *NFP* utilizes a *softer* notion of fingerprint matching by checking whether the model outputs match *changes in normalized-logits*. Specifically, for classification models $f(x; \theta)$ with logits $h(x; \theta)$ (see Eqn 1), where F is defined as:

$$F(x, \Delta x^i) \triangleq \varphi(x + \Delta x^i) - \varphi(x), \quad \varphi(x) \triangleq h(x; \theta) / \|h(x; \theta)\|,$$

where φ are the normalized logits. The logits are normalized so the DNN does not fit the Δy by making the weights arbitrarily large. Here, we use $D(x, \Delta x^i)$ as in (5). Note that here $\Delta y^{i,j} \in \mathbb{R}^K$.

Choosing Δy For our experiments, we choose the Δy so that the normalized-logit of the true class either increases or decreases along the Δx^i (analogous to the linear case). For e.g., for a 10-class classification task, if x is in class k we choose Δy of the form: $\Delta y_{l \neq k}^k = \alpha$ and $\Delta y_{l=k}^k = -\beta$, for $k = 1, \dots, 10$, and $\alpha, \beta \in \mathbb{R}^+$. We found that reasonable choices are $\alpha = 0.25$ and $\beta = 0.75$, and that the method is not sensitive to these choices. For investigation in the grey-box setting (with an adaptive attacker), we randomize the Δy^k in addition to the Δx . This randomization minimizes the assumptions the attacker can make about the fingerprints and is detailed in Appendix C.

Choosing Δx For nonlinear models (e.g., DNNs), the best fingerprint-direction Δx choice is not clear. We use a straightforward extension from the linear case with randomly sampled Δx 's. Randomization minimizes structural assumptions that may make *NFP* exploitable. For all experiments, we sampled Δx^i uniformly from $[-\varepsilon, \varepsilon]^l$: $\Delta x^i \sim \mathcal{U}(-\varepsilon, \varepsilon)^l$, where l is the input dimension. Our experiments (see Figure 7) suggest that *NFP* is *not sensitive* to the random values sampled. This also suggests that the Δx^i could be chosen based on different approaches.

Visualizing Fingerprints. To understand the behavior for non-linear models, we trained a DNN (two hidden layers with 200 ReLU nodes each) to distinguish between two Gaussian balls in 2D spac. Figure 3 describes this experiment. Without fingerprints, the model learns an almost linear boundary separating the two balls (compare with Figure 2). When we train to encode the fingerprints, we observe that *NFP* causes the model to learn a non-linear pockets of low fingerprint-loss characterizing the data-distribution. In this simple setting, *NFP* learns to delineate the data-distribution, where the darker regions are accepted as real and the rest is rejected.

Source \ Dataset	Natural (FGSM)	Advers. (FGSM)	<i>NFP</i> (FGSM)	Natural (BIM-b)	Advers. (BIM-b)	<i>NFP</i> (BIM-b)
MNIST	99.96	99.91	99.32	99.62	99.77	99.83
CIFAR-10	99.92	99.89	99.43	99.71	99.41	99.35

Table 2: *NFP* detection AUC-ROC against *black-box attackers* (know dataset but not model or fingerprints), on MNIST, CIFAR-10 tasks on test-set (“real”) and corresponding black-box adversarial (“fake”) samples (1328 *pre-test* samples each). *NFP* achieves near perfect AUC-ROC. For CIFAR-10, the hyperparameters are $(N, \varepsilon) = (30, 0.003)$. For MNIST, $(N, \varepsilon) = (10, 0.03)$.

3.3 Threat Model Analysis for Adversarial Attacks

In the adversarial setting, the various threat-models describe varying amounts of information available to the attacker. We study *NFP* under multiple such threat models (Table 1), where the attacker has varying levels of knowledge of *NFPdata* and model $f(x; \theta)$.

In the **black-box attack setting** the attacker has no knowledge of the network weights *NFPdata*. We study *NFP* in this setting, and discuss query and transfer based attacks.

In the **grey-box** setting, the attacker has access to θ , can query $f(x; \theta)$ and its derivatives, *but does not know NFPdata*. We assume the adversary has access to the distribution from which the fingerprints are sampled but not the exact sequence of the fingerprints. This is a frequently used threat-model in cryptography and in practice, where a key or a password is used to secure a system. This setting is the most commonly studied, and is the focus of most defenses reported in Section 2 (e.g., [26, 18, 28]).

The grey-box setting is relevant, for instance, when the attacker has a copy of the classifier, but the fingerprints are private, in accordance with Kerchhoff’s principle [36] (e.g. when *NFP* is run on a cloud). We study grey-box attacks in detail because of its practical relevance, and show that safe-keeping of the fingerprints ensures robustness against adversarial attacks.

We note that reverse engineering the *NFPdata* by brute-force search can be combinatorially hard. To see this, consider a simple setting where only the $\Delta y^{i,j}$ are unknown, and that the attacker knows that each fingerprint is discrete, i.e. each component $\Delta y_k^{i,j} = \pm 1$. Then the attacker would have to search over combinatorially ($\mathcal{O}(2^{NK})$) many Δy to find the subset of Δy that satisfies the detection criterion in (6). Further, smaller τ s reduce the volume of inputs accepted as real. In our investigation in the grey-box setting, we randomize both the set of Δx s and the Δy s, thereby minimizing the structural assumptions the adversary can make with regard to the fingerprints.

The *strongest* threat model assumes the attacker has full information about the defender, for e.g., when the attacker can either reverse-engineer or has access to the fingerprint data *NFPdata*, so that stronger attacks could be possible. In this setting, *NFP* is robust to the full range of attacks in literature. However, we find that a new attack that adaptively solves the multi-objective optimization problem of minimizing the fingerprint-loss while producing a misclassification is able to fool *NFP* at large computational costs. We discuss the evaluation in detail under this setting in Appendix F.

Additionally, we define the notion of **white-box defense** (defender is aware of the attack mechanism) and **black-box defense** (defender has no knowledge about attacker) – *NFP* is a black-box defense. There has been considerable progress in black-box attack and white-box defense settings (e.g. [37]). However, progress in grey-box attack, black-box defense threat-models is relatively limited.

4 Experiments

We empirically validate *NFP* on a number of vision data-sets, We analyze the behavior and robustness of *NFP* against adversarial attacks under various threat models. We also study the sensitivity of *NFP* to varying hyperparameters. The study of the white-box-attack setting is deferred to Appendix F. We empirically find that:

- *NFP* is robust under the black-box and grey-box adversarial threat-models.

Data	Method	FGSM	JSMA	BIM-a	BIM-b	CW- L_2
MNIST	LID	99.68	96.36	99.05	99.72	98.66
	KD	81.84	66.69	99.39	99.84	96.94
	BU	27.21	12.27	6.55	23.30	19.09
	KD+BU	82.93	47.33	95.98	99.82	85.68
	<i>NFP</i>	100.0	99.97	99.94	99.98	99.74
CIFAR-10	LID	82.38	89.93	82.51	91.61	93.32
	KD	62.76	84.54	69.08	89.66	90.77
	BU	71.73	84.95	82.23	3.26	89.89
	KD+BU	71.40	84.49	82.07	1.1	89.30
	<i>NFP</i>	99.96	99.91	99.91	99.95	98.87

Table 3: Detection AUC-ROC of black-box defenders (do not know attack strategy) against *partial-white-box-attackers* (know model $f(x; \theta)$, but not defense details; see Section 3.3), on MNIST, CIFAR-10 on test-set (“real”) and corresponding adversarial (“fake”) samples (1328 *pre-test* samples each). *NFP* outperforms baselines (LID, KD, BU) on MNIST & CIFAR-10.

- Using *NFP* does not diminish prediction accuracy (when not abstaining).

Adversarial Attacks We perform evaluation against adversarial attacks under various threat-models on the MNIST, CIFAR-10 and MiniImagenet-20 datasets. We use the following state-of-the-art attacks (Table 12):

- *Fast Gradient Method* (FGSM) [6] and *Basic Iterative Method* (BIM) [38] are both gradient based attacks with BIM being an iterative variant of FGSM. We consider both BIM-a (iterates until misclassification has been achieved) and BIM-b (iterates 50 times).
- *Jacobian-based Saliency Map Attack* (JSMA) [39] perturbs pixels using a saliency map.
- *Carlini-Wagner Attack* (CW- L_2): an attack that optimizes to minimize the perturbation needed for misclassification, and is one of the strongest known attacks [40, 22].

On CIFAR-10 and MiniImagenet-20, all attacks have a successful misclassification rate of 99 – 100% and on MNIST, FGSM has a successful misclassification rate of 89%, while the other attacks have near-perfect misclassification rates. See Table 12 for attack success rates and distortion bounds.

4.1 Black-box adversarial Examples

We consider black-box adversarial examples on MNIST and CIFAR-10. Even though the black-box setting is the weakest threat model, practical black-box attacks have been shown to be feasible in several real-world applications [41, 42].

MNIST. We train a 5-layer ConvNet to $99.2 \pm 0.1\%$ test-accuracy. The set of $\Delta x^i \in \mathbb{R}^{28 \times 28}$ is chosen randomly, with each value chosen uniformly in $[-\varepsilon, \varepsilon]$. For each Δx^i , if x is of label-class k , $\Delta y^{i,k} \in \mathbb{R}^{10}$ is chosen to be such that $\Delta y_{l \neq k}^{i,k} = 0.25$ and $\Delta y_{l=k}^{i,k} = -0.75$, with $\|\Delta y\|_2 = 1$.

CIFAR-10. For CIFAR-10, we trained a 7-layer ConvNet (similar to [40]) to $85 \pm 1\%$ accuracy. The Δx^i and $\Delta y^{i,j}$ are chosen similarly as for MNIST.

First, we consider transfer based attacks [41] from models trained i) naturally, ii) adversarially using robust learning, and iii) with *NFP*. The results are summarized in Table 2, and we see that *NFP* is able to detect transfer based attacks with near-perfect accuracy. Next, we consider query based attacks such as [43, 44]. A key first step for these attacks is the ability to sample adversarial points that can fool the detector. To evaluate the feasibility of such attacks on *NFP*, we sample large numbers of points randomly and check if they are adversarial. We see that from over 10^9 sampled points (with relatively large perturbations), we do not encounter a single adversarial point with a small fingerprint loss (See Appendix E for details).

We finally consider an attack where the adversary has access to the distribution from which the fingerprints are sampled but not the exact fingerprints nor the model weights. Under this scenario, the adversary can attack an ensemble of models trained with *NFP* by sampling fingerprints from the distribution and exploit the transferability of adversarial examples to attack the original model. We train an ensemble of three substitute models, and generate adversarial examples using the white-box-

Data	Unknown Δx , Unknown Δy	Unknown Δx , known Δy
CIFAR-10	100.00	99.85

Table 4: Detection AUC-ROC of *NFP* vs grey-box EOT attacks (100 pre-test samples).

attack described in Appendix F. For this attack, 45.1% of the adversarial examples do not transfer, and *NFP* achieves an AUC-ROC of 94.72% on the remaining samples.

4.2 Grey-box adversarial Examples

This threat-model is considerably stronger than the black-box setting. The adversary has access to the model weights and the distribution from which the fingerprints are sampled. The baselines LID [26], a recent detection based defense; KD; BU [27]; all trained on FGSM, as in [26] evaluate primarily in this setting. Following [26], for each dataset we consider a randomly sampled *pre-test*-set of unseen 1328 test-set images, and discard misclassified pre-test images. For the *test-set* of remaining images, we generate adversarial perturbations by applying each of the above mentioned attacks. We report AUC-ROC on sets composed in equal parts of the *test-set* and *test-set* adversarial samples. The AUC-ROC is computed by varying the threshold τ . See Appendix for model and dataset details.

The FGSM, BIM-a, BIM-b and JSMA attacks are untargeted. We use published code for the attacks and code from [26] for the baselines. The AUC-ROCs for the best N and ε using grid-search are reported in Table 3. We see that *NFP* achieves near-perfect detection with AUC-ROC of 99 – 100% across all attacks. On CIFAR-10, across attacks, *NFP* outperforms LID on average by **11.77%** and KD+BU, KD, BU even more substantially (Table 3). Even compared to LID-white-box (where LID is aware of the attackers mechanism but *NFP* is not), *NFP* outperforms LID-white-box on average by **8.0%** (Appendix, Table 10). Further, we find that *NFP* is robust across a wide-range of hyperparameter choices. (See Figures 5,7). Additionally, we evaluated *NFP* against Wasserstein Adversarial Examples, introduced recently in [45]. *NFP* is able to distinguish between adversarial and clean data with an 98%+ AUC-ROC (See Appendix for details). Wasserstein adversarial examples include perturbations such as scaling, rotation, translation, and distortion.

MiniImagenet-20. We test on *MiniImagenet-20* with 20 classes randomly chosen (from 100) [46] and trained an AlexNet network on 10,600 images (not downsampled) with 91.1% top-1 accuracy. We generated test-set adversarial examples using BIM-b with 50 steps [47] and FGSM. *NFP* achieves AUC-ROCs of > 99.5% (Table 5). We could not get results for JSMA and CW- L_2 , which require too much computation for tasks of this size. Results for other defenses are not reported due to unavailable implementations.

Data	FGSM	BIM-b
MiniImagenet-20	99.96	99.68

Table 5: AUC-ROC of *NFP* vs *grey-box attacks* on MiniImagenet-20, $(N, \varepsilon) = (20, 0.05)$.

A more sophisticated grey-box attack is one where the adversary attempts to use the fingerprint distribution from which the fingerprints are sampled from to mount an adaptive attack. We investigate the robustness of *NFP* against such an attacker. For this setup, we randomize both the Δy s and the Δx s (See Appendix C for details). Several defenses relying on randomness [24, 16] have been rendered vulnerable using the expectation-over-transformation (EOT) attack introduced in [20]. Under this attack, we consider two scenarios: (i) the adversary has access to the exact Δy but not Δx , and (ii) the adversary does not have access to both the Δx , Δy . Note that scenario (i) is not likely in practice, but we evaluate to consider how much information an attacker needs to render *NFP* vulnerable. In scenario (ii), the adversary attempts to minimize the fingerprint-loss in expectation while producing a misclassification on the original model by minimizing the following objective:

$$L_{adv}(x, y^*, \theta) + \gamma \mathbb{E}_{\Delta x \sim T_{\Delta x}, \Delta y \sim T_{\Delta y}} [L_{fp}(x, y^*, \chi; \theta)],$$

where L_{adv} is the misclassification objective, $T_{\Delta x}$ and $T_{\Delta y}$ are the distributions from which Δx and Δy are sampled respectively. To mount the EOT attack, at each iteration, the adversary samples a new set of fingerprints and attempts to minimize the fingerprint-loss while producing a misclassification. For this, we use the attack that is successful in the white-box setting described in Appendix F for 50000 steps. Attacks for the other scenarios are constructed similarly. The results for these attacks are summarized in Table 4, and we find that the defense is robust against the EOT attack.

5 Conclusion

Our experiments suggest *NFP* is efficient at safeguarding DNNs from adversarial attacks. We find that *NFP* is effective at detecting the full range of state-of-the-art adversarial attacks (grey/black-box), and the high AUC-ROC scores indicate that the fingerprints generalize well to the test-set, but not to adversarial examples. Furthermore, we find that *NFP* is robust to a full-range of white-box attacks available in literature; we then develop a new attack to fool *NFP*, pushing white-box attacks further.

References

- [1] Kaiming He, Xiangyu Zhang, Shaoqing Ren, and Jian Sun. Delving deep into rectifiers: Surpassing human-level performance on imagenet classification. *CoRR*, abs/1502.01852, 2015.
- [2] Wayne Xiong, Jasha Droppo, Xuedong Huang, Frank Seide, Mike Seltzer, Andreas Stolcke, Dong Yu, and Geoffrey Zweig. Achieving human parity in conversational speech recognition. *CoRR*, abs/1610.05256, 2016.
- [3] David Silver, Aja Huang, Chris J. Maddison, Arthur Guez, Laurent Sifre, George van den Driessche, Julian Schrittwieser, Ioannis Antonoglou, Veda Panneershelvam, Marc Lanctot, Sander Dieleman, Dominik Grewe, John Nham, Nal Kalchbrenner, Ilya Sutskever, Timothy Lillicrap, Madeleine Leach, Koray Kavukcuoglu, Thore Graepel, and Demis Hassabis. Mastering the game of Go with deep neural networks and tree search. *Nature*, 529(7587):484–489, January 2016.
- [4] Anh Mai Nguyen, Jason Yosinski, and Jeff Clune. Deep neural networks are easily fooled: High confidence predictions for unrecognizable images. In *IEEE Conference on Computer Vision and Pattern Recognition, CVPR*, pages 427–436, 2015.
- [5] Christian Szegedy, Wojciech Zaremba, Ilya Sutskever, Joan Bruna, Dumitru Erhan, Ian Goodfellow, and Rob Fergus. Intriguing properties of neural networks. *arXiv preprint arXiv:1312.6199*, 2013.
- [6] Ian J. Goodfellow, Jonathon Shlens, and Christian Szegedy. Explaining and harnessing adversarial examples. *CoRR*, abs/1412.6572, 2014.
- [7] Michael Felderer, Matthias Büchler, Martin Johns, Achim D. Brucker, Ruth Breu, and Alexander Pretschner. Security testing: A survey. In *Chapter One*, volume 101 of *Advances in Computers*, pages 1–51. Elsevier, 2016.
- [8] Mohd Ehmer and Farmeena Khan. A comparative study of white box, black box and grey box testing techniques. *International Journal of Advanced Computer Science and Applications*, 3, 6 2012.
- [9] Ludwig Schmidt, Shibani Santurkar, Dimitris Tsipras, Kunal Talwar, and Aleksander Madry. Adversarially robust generalization requires more data. *CoRR*, abs/1804.11285, 2018.
- [10] Dimitris Tsipras, Shibani Santurkar, Logan Engstrom, Alexander Turner, and Aleksander Madry. Robustness may be at odds with accuracy. In *International Conference on Learning Representations*, 2019.
- [11] A. Raghunathan, J. Steinhardt, and P. Liang. Certified Defenses against Adversarial Examples. *ArXiv e-prints*, January 2018.
- [12] J. Zico Kolter and Eric Wong. Provable defenses against adversarial examples via the convex outer adversarial polytope. *CoRR*, abs/1711.00851, 2017.
- [13] A. Madry, A. Makelov, L. Schmidt, D. Tsipras, and A. Vladu. Towards Deep Learning Models Resistant to Adversarial Attacks. *ArXiv e-prints*, June 2017.
- [14] Yash Sharma and Pin-Yu Chen. Attacking the madry defense model with ℓ_1 -based adversarial examples, 2018.
- [15] Yang Song, Rui Shu, Nate Kushman, and Stefano Ermon. Constructing unrestricted adversarial examples with generative models. In S. Bengio, H. Wallach, H. Larochelle, K. Grauman, N. Cesa-Bianchi, and R. Garnett, editors, *Advances in Neural Information Processing Systems 31*, pages 8322–8333. Curran Associates, Inc., 2018.
- [16] Cihang Xie, Jianyu Wang, Zhishuai Zhang, Zhou Ren, and Alan Yuille. Mitigating adversarial effects through randomization. *International Conference on Learning Representations*, 2018.

- [17] Jacob Buckman, Aurko Roy, Colin Raffel, and Ian Goodfellow. Thermometer encoding: One hot way to resist adversarial examples. *International Conference on Learning Representations*, 2018.
- [18] Yang Song, Taesup Kim, Sebastian Nowozin, Stefano Ermon, and Nate Kushman. Pixeldefend: Leveraging generative models to understand and defend against adversarial examples. *International Conference on Learning Representations*, 2018.
- [19] Rama Chellappa Pouya Samangouei, Maya Kabkab. Defense-GAN: Protecting classifiers against adversarial attacks using generative models. *International Conference on Learning Representations*, 2018.
- [20] Anish Athalye, Nicholas Carlini, and David Wagner. Obfuscated gradients give a false sense of security: Circumventing defenses to adversarial examples. In *Proceedings of the 35th International Conference on Machine Learning, ICML 2018*, July 2018.
- [21] Jonathan Uesato, Brendan O’Donoghue, Pushmeet Kohli, and Aaron van den Oord. Adversarial risk and the dangers of evaluating against weak attacks. In Jennifer Dy and Andreas Krause, editors, *Proceedings of the 35th International Conference on Machine Learning*, volume 80 of *Proceedings of Machine Learning Research*, pages 5025–5034, Stockholm, Sweden, 10–15 Jul 2018. PMLR.
- [22] Nicholas Carlini and David A. Wagner. Adversarial examples are not easily detected: Bypassing ten detection methods. *CoRR*, abs/1705.07263, 2017.
- [23] Dongyu Meng and Hao Chen. Magnet: a two-pronged defense against adversarial examples. *CoRR*, abs/1705.09064, 2017.
- [24] Chuan Guo, Mayank Rana, Moustapha Cisse, and Laurens van der Maaten. Countering adversarial images using input transformations. In *International Conference on Learning Representations*, 2018.
- [25] Nicholas Carlini and David A. Wagner. Magnet and "efficient defenses against adversarial attacks" are not robust to adversarial examples. *CoRR*, abs/1711.08478, 2017.
- [26] Xingjun Ma, Bo Li, Yisen Wang, Sarah M. Erfani, Sudanthi Wijewickrema, Grant Schoenebeck, Michael E. Houle, Dawn Song, and James Bailey. Characterizing adversarial subspaces using local intrinsic dimensionality. *International Conference on Learning Representations*, 2018. accepted as oral presentation.
- [27] R. Feinman, R. R. Curtin, S. Shintre, and A. B. Gardner. Detecting Adversarial Samples from Artifacts. *ArXiv e-prints*, March 2017.
- [28] K. Lee, K. Lee, H. Lee, and J. Shin. A Simple Unified Framework for Detecting Out-of-Distribution Samples and Adversarial Attacks. *Advances in Neural Information Processing Systems 31*, December 2018.
- [29] Nicholas Carlini and David A. Wagner. Audio adversarial examples: Targeted attacks on speech-to-text. *CoRR*, abs/1801.01944, 2018.
- [30] R. Jia and P. Liang. Adversarial examples for evaluating reading comprehension systems. In *Empirical Methods in Natural Language Processing (EMNLP)*, 2017.
- [31] Kathrin Grosse, Nicolas Papernot, Praveen Manoharan, Michael Backes, and Patrick McDaniel. Adversarial examples for malware detection. In Simon N. Foley, Dieter Gollmann, and Einar Snekkenes, editors, *Computer Security – ESORICS 2017*, pages 62–79, Cham, 2017. Springer International Publishing.
- [32] Blaine Nelson, Marco Barreno, Fuching Jack Chi, Anthony D. Joseph, Benjamin I. P. Rubinstein, Udam Saini, Charles Sutton, J. D. Tygar, and Kai Xia. Exploiting machine learning to subvert your spam filter. In *Proceedings of the 1st Usenix Workshop on Large-Scale Exploits and Emergent Threats*, LEET’08, pages 7:1–7:9, Berkeley, CA, USA, 2008. USENIX Association.
- [33] David Wagner and Paolo Soto. Mimicry attacks on host-based intrusion detection systems. In *Proceedings of the 9th ACM Conference on Computer and Communications Security, CCS ’02*, pages 255–264, New York, NY, USA, 2002. ACM.
- [34] Scott Alfeld, Xiaojin Zhu, and Paul Barford. Data poisoning attacks against autoregressive models. In *Proceedings of the Thirtieth AAAI Conference on Artificial Intelligence, AAAI’16*, pages 1452–1458. AAAI Press, 2016.

- [35] N. Akhtar and A. Mian. Threat of adversarial attacks on deep learning in computer vision: A survey. *IEEE Access*, 6:14410–14430, 2018.
- [36] C. E. Shannon. Communication theory of secrecy systems. *The Bell System Technical Journal*, 28(4):656–715, October 1949.
- [37] Fangzhou Liao, Ming Liang, Yinpeng Dong, Tianyu Pang, Jun Zhu, and Xiaolin Hu. Defense against adversarial attacks using high-level representation guided denoiser. *CoRR*, abs/1712.02976, 2017.
- [38] Alexey Kurakin, Ian J. Goodfellow, and Samy Bengio. Adversarial examples in the physical world. *CoRR*, abs/1607.02533, 2016.
- [39] Nicolas Papernot, Patrick D. McDaniel, Somesh Jha, Matt Fredrikson, Z. Berkay Celik, and Ananthram Swami. The limitations of deep learning in adversarial settings. *CoRR*, abs/1511.07528, 2015.
- [40] N. Carlini and D. Wagner. Towards Evaluating the Robustness of Neural Networks. *ArXiv e-prints*, August 2016.
- [41] Nicolas Papernot, Patrick D. McDaniel, and Ian J. Goodfellow. Transferability in machine learning: from phenomena to black-box attacks using adversarial samples. *CoRR*, abs/1605.07277, 2016.
- [42] Nicolas Papernot, Patrick McDaniel, Ian Goodfellow, Somesh Jha, Z. Berkay Celik, and Ananthram Swami. Practical black-box attacks against machine learning. In *Proceedings of the 2017 ACM on Asia Conference on Computer and Communications Security, ASIA CCS '17*, pages 506–519, New York, NY, USA, 2017. ACM.
- [43] Andrew Ilyas, Logan Engstrom, Anish Athalye, and Jessy Lin. Black-box adversarial attacks with limited queries and information. In *Proceedings of the 35th International Conference on Machine Learning, ICML 2018*, July 2018.
- [44] Wieland Brendel, Jonas Rauber, and Matthias Bethge. Decision-based adversarial attacks: Reliable attacks against black-box machine learning models. In *International Conference on Learning Representations*, 2018.
- [45] Eric Wong, Frank R. Schmidt, and J. Zico Kolter. Wasserstein adversarial examples via projected sinkhorn iterations. *CoRR*, abs/1902.07906, 2019.
- [46] Oriol Vinyals, Charles Blundell, Tim Lillicrap, koray kavukcuoglu, and Daan Wierstra. Matching networks for one shot learning. In D. D. Lee, M. Sugiyama, U. V. Luxburg, I. Guyon, and R. Garnett, editors, *Advances in Neural Information Processing Systems 29*, pages 3630–3638. Curran Associates, Inc., 2016.
- [47] Google Brain. Nips 2017: Non-targeted adversarial attack, 2017. Accessed: 2017-02-07.

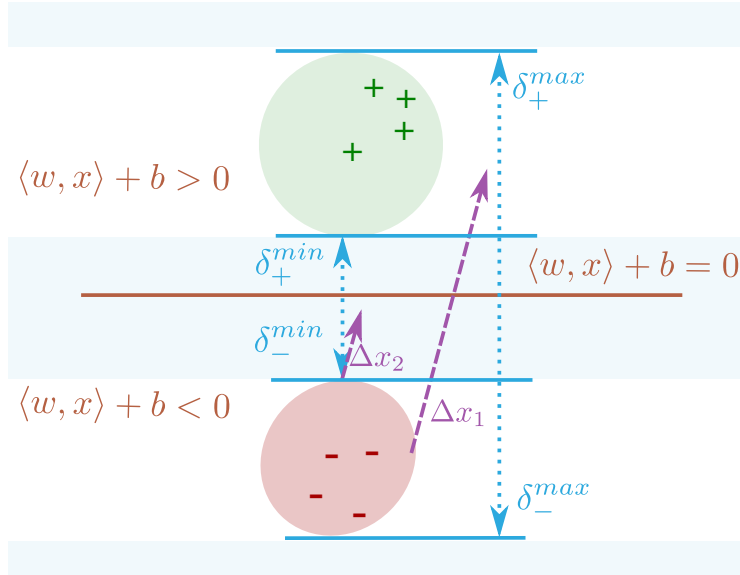


Figure 4: Geometry of fingerprints for SVMs with linearly separable data. Let $d(x)$ be the distance of x to the decision boundary (see Thm 1). δ_{\pm}^{max} (δ_{\pm}^{min}) denote the maximal (minimal) distances of the positive (x_+) and negative (x_-) examples to the separating hyperplane $\langle w, x \rangle + b = 0$. The fingerprint Δx^1 with $\langle \Delta x^1, e \rangle = \delta_-^{min}$ will have $f(x_- + \Delta x) < 0$ and $f(x_-) < 0$ for all x_- in the data distribution (red region). Hence, Δx^1 will flag all x' in the regions $-\delta_-^{min} < d(x') < 0$ as “fake”, since for those x' it will *always* see a change in predicted class. Similarly, Δx^2 with $\langle \Delta x^2, e \rangle = \delta_-^{max}$ always sees a class change for real x_- , thus flagging all x' with $d(x') < -\delta_-^{max}$ as “fake”.

Appendices

A Proof for Theorem 1

Proof. Also see Figure 4. Consider any perturbation $\eta = \lambda e$ that is positively aligned with w , and has $\langle \eta, e \rangle = \delta_-^{min}$. Then for any negative example $(x_-, -1)$ (except for the support vectors that lie exactly δ_-^{min} from the hyperplane), adding the perturbation η does not change the class prediction:

$$\text{sign } f(x_-) = -1, \quad \text{sign } f(x_- - \eta) = -1. \quad (12)$$

The fingerprint in (7) is an example of such an η . However, if λ is large enough, that is:

$$\langle \eta, e \rangle = \delta_-^{max}, \quad (13)$$

(e.g. the fingerprint in (8)), for *all* negative examples $(x_-, -1)$ the class prediction will *always* change (except for the x_- that lie exactly δ_-^{max} from the hyperplane):

$$\text{sign } f(x_-) = -1, \quad \text{sign } f(x_- + \eta) = +1, \quad (14)$$

Note that if η has a component smaller (or larger) than δ_{\pm}^{min} , it will exclude *fewer* (more) examples, e.g. those that lie closer to (farther from) the hyperplane. Similar observations hold for fingerprints (9) and (10) and the positive examples x_+ . Hence, it follows that for any x that lies too close to the hyperplane (closer than δ_{\pm}^{min}), or too far (farther than δ_{\pm}^{max}), the model output after adding the four fingerprints will never perfectly correspond to their behavior on examples x from the data distribution. For instance, for any x that is closer than δ_+^{min} to the hyperplane, (10) will always cause a change in class, while none was expected. Similar observations hold for the other regions in (11). Since the SVM is translation invariant parallel to the hyperplane, the fingerprints can only distinguish examples based on their distance perpendicular to the hyperplane. Hence, this choice of λ s is optimal. \square

Layer	Parameters
Convolution + ReLU + BatchNorm	$11 \times 11 \times 64$
MaxPool	3×3
Convolution + ReLU + BatchNorm	$5 \times 5 \times 192$
MaxPool	3×3
Convolution + ReLU + BatchNorm	$3 \times 3 \times 384$
MaxPool	3×3
Convolution + ReLU + BatchNorm	$3 \times 3 \times 256$
MaxPool	3×3
Convolution + ReLU + BatchNorm	$3 \times 3 \times 156$
MaxPool	3×3
Fully Connected + ReLU + BatchNorm	3072
Dropout	-
Fully Connected + ReLU + BatchNorm	1024
Dropout	-
Softmax	20

Table 6: MiniImagenet-20 Model Used

Layer	Parameters
Convolution + ReLU + BatchNorm	$5 \times 5 \times 32$
MaxPool	2×2
Convolution + ReLU + BatchNorm	$5 \times 5 \times 64$
MaxPool	2×2
Fully Connected + ReLU + BatchNorm	200
Fully Connected + ReLU + BatchNorm	200
Softmax	10

Table 7: MNIST Model Used

Layer	Parameters
Convolution + ReLU + BatchNorm	$3 \times 3 \times 32$
Convolution + ReLU + BatchNorm	$3 \times 3 \times 64$
MaxPool	2×2
Convolution + ReLU + BatchNorm	$3 \times 3 \times 128$
Convolution + ReLU + BatchNorm	$3 \times 3 \times 128$
MaxPool	2×2
Fully Connected + ReLU + BatchNorm	256
Fully Connected + ReLU + BatchNorm	256
Softmax	10

Table 8: CIFAR Model Used

B Models for Evaluation

Note: Code for CW-adaptive is based on code from https://github.com/carlini/nn_robust_attacks. We use published code from [45] for Wasserstein Adversarial Attack, and the other attacks were obtained from the paper [26].

B.1 MNIST

For MNIST, we use the model described in Table 7.

B.2 CIFAR-10

For CIFAR-10, we use the model described in Table 8

B.3 MiniImagenet-20

MiniAlexNet Model We use a model similar to AlexNet for MiniImagenet-20. The model used is described in Table 6

MiniImagenet-20 classes We use images from the following 20 ImageNet classes for our experiments:

n01558993, n02795169, n03062245, n03272010, n03980874, n04515003 n02110063, n02950826, n03146219, n03400231, n04146614, n04612504, n02443484, n02981792, n03207743, n03476684, n04443257, n07697537

C Grey-box Evaluation – Δy Hyperparameters

Instead of simple $\Delta y^{i,j}$, we can encode more complex fingerprints that are harder to guess for an adversary. For the grey-box threat-model evaluation in Section 4.2, for each Δx^i , we sample $\Delta y^{i,j} \in \mathbb{R}^{10}$ such that each entry of $\Delta y^{i,j}$ is uniformly drawn from $[-0.5, 0.5]$. This random sampling minimizes the structural assumptions the adversary can make about the fingerprints.

D Sensitivity analysis

We study the effect of changing N (number of fingerprint directions) and ε (magnitude of fingerprint-perturbation Δx) on the AUC-ROC for CIFAR-10 and MNIST. Figure 6 and 5 show that *NFP* performs well across a wide range of hyperparameters and is robust to variation in the hyperparameters for PWAs. With increasing ε , the AUC-ROC for CW- L_2 decreases. As discussed before, a possible explanation is that CW- L_2 produces smaller adversarial perturbations than other attacks, and for larger fingerprint-distortions ε , the fingerprints are less sensitive to those small adversarial perturbations. However, the degradation in performance is not substantial ($\sim 4 - 8\%$) as we increase ε over an order of magnitude. With increasing N , the AUC-ROC generally increases across attacks. We conjecture that larger sets of fingerprints can detect perturbations in more directions and results in better detection.

Figure 7 shows that *NFP* achieves mean AUC-ROC of 98% – 100% against all PWA, with standard deviation $< 1\%$. This suggests that *NFP* is *not very sensitive to the chosen fingerprints*.

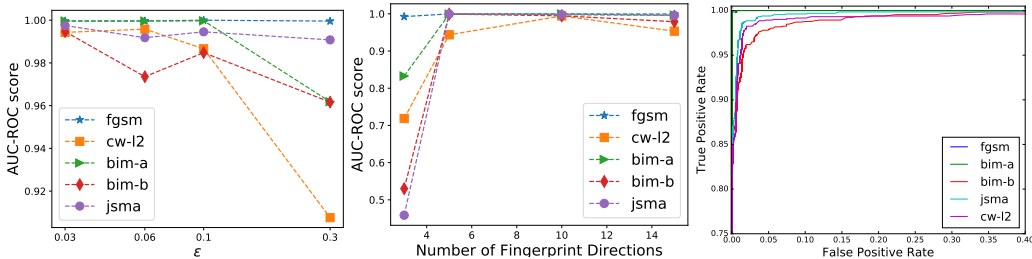


Figure 5: AUC-ROC performance for different hyperparameter settings (top-left: Varying ε ($N = 10$), top-right: Varying N ($\varepsilon = 0.03$)) and ROC curves (bottom) on MNIST. We see that the performance of *NFP* is robust across attacks and hyperparameters, with the AUC-ROC between 90 – 100% for most settings. The AUC-ROC is lowest versus CW- L_2 , which is one of the strongest known attack.

E Randomized Queries – sanity check for query based attacks

To evaluate the feasibility of query based black-box attacks such as [43, 44], we sample randomly in ε -balls around unseen test-data to find adversarial examples. For 100 MNIST test samples, we

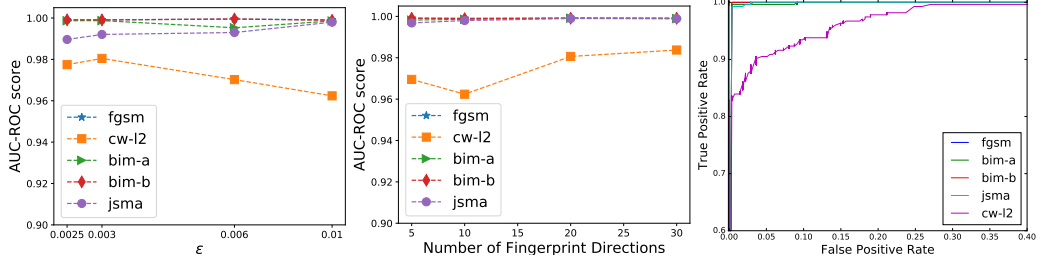


Figure 6: AUC-ROC for different hyperparameters (top-left: Varying fingerprint magnitude ϵ ($N = 10$), top-right: Varying no. fingerprints (N) ($\epsilon = 0.01$) and ROC curves (bottom) on CIFAR-10 for partial-whitebox attacks. For analysis on MNIST, see Appendix. *NFP* is robust across attacks & hyperparameters with an AUC-ROC between 95 – 100%. Increasing N improves performance, indicating more fingerprints are harder to fool. Increasing the magnitude ϵ decreases AUC on CW- L_2 only, suggesting that as adversarial perturbations become of smaller magnitude, *NFP* requires smaller ϵ .

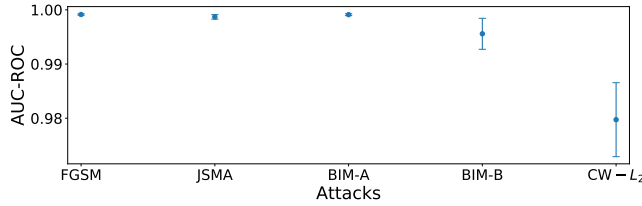


Figure 7: AUC-ROC mean μ and standard-deviation σ for 32 randomly sampled fingerprints (including randomizing N) for CIFAR-10. The AUC-ROC across all PWAs varies little ($\sigma < 1\%$), with σ highest for CW- L_2 .

sample 10^6 points uniformly from the l_∞ -ball with $\|\eta\|_\infty \leq 0.3$ and for 50 CIFAR-10 test samples, we sample 5×10^5 points uniformly from the l_∞ -ball with $\|\eta\|_\infty \leq 0.25$. Amongst these randomly sampled points for each test point, we compute the smallest $\min_i (L_{fp}(x, i, \xi; \theta))$ (let us call this value L_{fp}^*) across points that are adversarial (i.e. cause a misclassification). Note that L_{fp}^* for each test point is the minimum fingerprint-loss over all adversarial samples sampled around the point and across all labels. For CIFAR-10, we are able to find adversarial examples for 47 points and for MNIST, we are able to find adversarial examples for 52 points. Figure 8 shows the distribution of L_{fp} across the test points and L_{fp}^* across the corresponding randomly sampled adversarial points. We observe that for MNIST, one single test sample has a high fingerprint-loss while all adversarial samples have high fingerprint-losses. The remaining test-samples have fingerprint-losses that are roughly 3 – 30 times smaller than the adversarial examples. For CIFAR-10, the test and adversarial points are well separated, with most test samples having losses significantly smaller (roughly 10 times smaller) than the randomly sampled adversarial examples. This indicates that it is extremely difficult to perform query based black-box adversarial attacks against *NFP*. This also indicates that *NFP* removes most of the adversarial examples, and does not simply gradient mask.

F Whitebox Analysis of *NFP*

The strongest threat-model, whitebox-attack, is one where the adversary has access to the parameters of *NFP*. To evaluate whether *NFP* is robust in this setting, we consider adaptive variants of FGSM, BIM-b, CW- L_2 , and SPSA [21]. Under this threat-model the attacker tries to find an adversarial example x' that also minimizes the fingerprint-loss (3), while attacking the model trained with *NFP*. We find that *NFP* is robust across the full range of such state-of-the-art attacks, achieving AUC-ROCs of 96-100% (See Table 9)

Adaptive-FGSM, Adaptive-BIM-b, Adaptive-SPSA For the FGSM, BIM-b and SPSA (untargeted) attacks we mount an adaptive attack with a modified optimization objective as in [21]. Specifi-

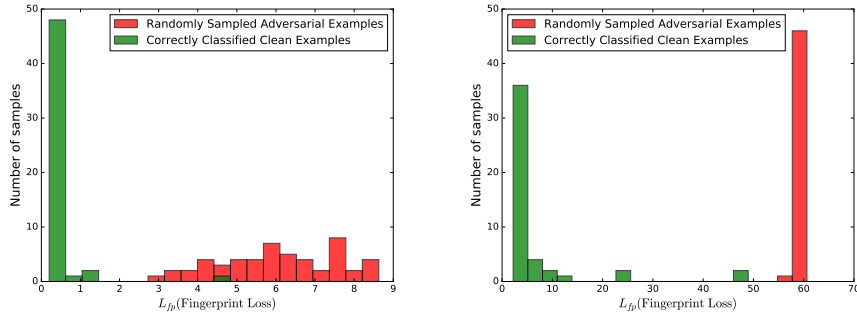


Figure 8: Top: MNIST, Bottom: CIFAR-10. Histograms depicting the distribution of losses for randomly sampled adversarial examples and test-data. Randomly sampled adversarial examples are well separated from unseen test examples. For *NFP*, hyperparameters are $(\epsilon, N) = (0.1, 10)$ and $(\epsilon, N) = (0.003, 30)$ for MNIST and CIFAR-10 respectively.

Data	Method	Adaptive-FGSM	Adaptive-BIM-b	Adaptive-CW- L_2	Adaptive-CW- L_2 ($\gamma_2 = 1$)	Adaptive-SPSA
MNIST	<i>NFP</i>	99.91	99.37	95.04	99.17	99.94
CIFAR-10	<i>NFP</i>	99.99	99.92	97.19	97.56	99.99

Table 9: Detection AUC-ROC for adaptive whitebox attacks on datasets MNIST and CIFAR-10. Other defenses such as [18, 37], including the baselines KD and BU, fail under adaptive-attacks ($< 10\%$ accuracy). For MNIST, the *NFP* parameters for FGSM, SPSA are $(\epsilon, N) = (0.1, 10)$ and $(\epsilon, N) = (0.05, 20)$ for the BIM-b, CW- L_2 attacks. For CIFAR-10, the parameters are set at $(\epsilon, N) = (0.003, 30)$ across attacks.

cally, for SPSA, the loss function to minimize is:

$$J_{\theta}^{\text{adv}}(x', y^*, \theta) + \gamma L_{\text{fp}}(x', y^*, \chi; \theta),$$

where J_{θ}^{adv} is the original adversarial objective from [21]. For the gradient-based FGSM and BIM-B attacks, we use gradients of the following loss function:

$$L_{CE}(x, y^*, \theta) - \gamma L_{\text{fp}}(x, y^*, \chi; \theta),$$

where $L_{CE}(x, y^*)$ is the cross-entropy loss. For each of the attacks and for each data-point, we choose the largest $\gamma \in [10^{-3}, 10^4]$ that results in a successful attack with a bisection search over γ – note that larger γ values increase the priority for minimizing L_{fp} . For the three adaptive attacks, the perturbation bounds are $\|\eta\|_{\infty} \leq 0.4$ for MNIST and $\|\eta\|_{\infty} \leq 0.05$ for CIFAR-10.

Adaptive-CW- L_2 We consider two adaptive variants of the CW- L_2 attack. The first variant we consider is with the modified objective function:

$$\min_{x'} \|x - x'\|_2 + \gamma_1 (L_{\text{CW}}(x') + \gamma_2 L_{\text{fp}}(x', y^*, \chi; \theta)). \quad (15)$$

Here, y^* is the label-vector, $\gamma_1 \in [10^{-3}, 10^6]$ and $\gamma_2 \in [10^{-3}, 10^4]$ are scalar coefficients, L_{fp} is the fingerprint-loss we trained on and L_{CW} is an objective encouraging misclassification. To find γ_1 and γ_2 we do a bisection search, first decreasing γ_1 (as in [22]) and then increasing γ_2 gradually in a similar manner. Note that increasing γ_2 increases the importance given to minimizing L_{fp} . The successful attack with the smallest L_{fp} during our search is chosen.

The second variant is similar to the one considered in [22]. Here γ_2 is held at 1.0 and the successful attack with the smallest $\|x - x'\|_2$ is chosen during a bisection search over γ_1 .

F.1 New White-Box Attack for Breaking *NFP*

While *NFP* is robust to the full range of attacks studied above, we find that this is because of the highly nonconvex problem the attacker is required to solve. During detailed analysis we notice that during the multi-objective optimization of minimizing the fingerprint loss (L_{fp}) and the misclassification loss (L_{adv}), the individual losses oscillate, which makes it difficult to craft adversarial examples with

Data	Method	FGM	JSMA	BIM-a	BIM-b	CW- L_2
MNIST	LID	99.68	98.67	99.61	99.90	99.55
	<i>NFP</i>	100.0	99.97	99.94	99.98	99.74
CIFAR-10	LID	82.38	95.87	82.30	99.78	98.94
	<i>NFP</i>	99.96	99.91	99.91	99.95	98.87

Table 10: Detection AUC-ROC for *NFP*, whitebox-LID against *whitebox-attackers* (know model $f(x; \theta)$, but not fingerprints; see Section 3.3), on MNIST, CIFAR-10 tasks on test-set (“real”) and corresponding adversarial (“fake”) samples (1328 *pre-test* samples each). *NFP* outperforms the baselines (LID, KD, BU) on MNIST and CIFAR-10 across all attacks, except CW- L_2 where it performs comparably. A possibly explanation for LID’s improved performance against stronger, iterative attacks is gradient masking [20].

Method	Parameters
CW- $L - 2$	Bisection-steps (γ_1)=9, Bisection-steps (γ_2)=5, Max Iteration Steps = 1000, L2_ABORT_EARLY = True, L2_LEARNING_RATE = 1e-2, L2_TARGETED = True, L2_CONFIDENCE = 0, L2_INITIAL_CONST = 1e-3 (γ_1 initial value) L2_INITIAL_CONST_2 = 0.1 (γ_2 initial value)
SPSA	Bisection steps=6, Upper-bound for bisection = 50.0, spsa-iters=1, spsa-samples=128, Lower-bound=0.001 Iterations = 100, lr=0.01, dr=0.01
BIM (MNIST)	eps-iter=0.010
BIM (CIFAR)	eps-iter=0.005
Wasserstein (CIFAR)	Regularization=3000, Wasserstein-distance(p)=2, PGD Step Size(alpha)=0.1, epsilon=0.01, epsilon_factor=1.17, maxiters=400

Table 11: Attack hyperparameters corresponding to Tables 3,9, and 13.

low fingerprint loss. To solve this problem, we consider a new attack that can adaptively solve this optimization problem stabilizing the two losses and generating adversarial examples that successfully fool *NFP*.

Unlike current adaptive attacks which use a fixed coefficient (γ) when attacking detection models with multiple loss (e.g.: L_{fp} and L_{adv} in *NFP*), we scale both losses to balance the gradients from the two losses and simultaneously optimize both of them. To do this, we introduce two functions that vary monotonically as a function of the difference between the fingerprint-loss of the adversarial sample (x') and the real sample (x). Define $\Delta L_{fp}(x, x') = L_{fp}(x', y', \chi; \theta) - L_{fp}(x, y, \chi; \theta)$, where $y' = f(x')$. Define two functions:

$$f_1(x', x) := 10^{\Delta L_{fp}(x, x')},$$

and

$$f_2(x', x) := 0.1^{\Delta L_{fp}(x, x')},$$

We then perform an optimization based attack (with SGD) to minimize:

$$f_1(x', x)L_{fp}(x', y', \chi; \theta) + L_{adv}f_2(x', x).$$

We find that this cost function effectively optimizes both losses simultaneously, both producing a misclassification and minimizing the fingerprint-loss, thereby fooling the detector. Using this attack (50000 steps with learning-rate=0.00001) with a distortion bound of $\|\eta_\infty\| \leq 0.031$, we are able to reduce the AUC-ROC to about 0.5. This implies that the adversarial examples are virtually indistinguishable from real samples. We use this successful whitebox-attack to evaluate EOT and transfer based attacks in the grey-box/black-box setting.

G Attack Hyperparameters

Tables 11, 12 summarize the hyperparameter settings corresponding to the experiments in Tables 3,9, and 13.

Data	Attack	Test Accuracy	Bound on Adversarial Perturbation η
MNIST	FGSM	11.87%	$\ \eta\ _\infty \leq 0.4$
	BIM-a	0.00%	$\ \eta\ _\infty \leq 0.4$
	BIM-b	0.00%	$\ \eta\ _\infty \leq 0.4$
	JSMA	1.73%	
	CW- L_2	0.00%	
CIFAR	FGSM	11.39 %	$\ \eta\ _\infty \leq 0.05$
	BIM-a	0.00%	$\ \eta\ _\infty \leq 0.05$
	BIM-b	0.00%	$\ \eta\ _\infty \leq 0.05$
	JSMA	13.33%	
	CW- L_2	0.00%	
	Wasserstein	9.08%	
MiniImagenet	FGSM	0.00%	$\ \eta\ _\infty \leq 16/255$
	BIM-b	0.00%	$\ \eta\ _\infty \leq 16/255$

Table 12: Parameters and model test-accuracy on PW-attacks for different datasets (without *NFP* test). CW- L_2 , Wasserstein and JSMA attacks are unbounded. The bounds are relative to images with pixel intensities in $[0, 1]$.

Data	Attack	AUC-ROC
CIFAR-10	Wasserstein	98.14

Table 13: Detection AUC-ROC for *NFP* against greybox Wasserstein adversarial attack on CIFAR-10 task.

H Wasserstein Adversarial Example

NFP is able to distinguish between Wasserstein Adversarial Example and clean-data efficiently (Table 13). We increase the default epsilon value from 0.001 to 0.01 to achieve more than 90% attack success rate. The remaining hyperparameters are the same as in [45].